International Journal of GEOMATE, April, 2022, Vol.22, Issue 92, pp.64-70
ISSN: 2186-2982 (P), 2186-2990 (O), Japan, DOI: https://doi.org/10.21660/2022.92.7521
Geotechnique, Construction Materials and Environment

FRACTURE STIMULATION OF THE ADHESIVE POST-INSTALLED ANCHOR APPLIED TO EXISTING CONCRETE STRUCTURES

Takuma Kadono[1], *Shinichiro Okazaki[2], Taro Nakamura[3] and Mao Kurumatani[4]

[1]Graduate School of Engineering, Kagawa University, Japan; [2]Faculty of Engineering and Design, Kagawa University, Japan, [3]Yonden Consultants co., Inc., Japan,[4]Department of Urban and Civil Engineering, Ibaraki University, Japan

*Corresponding Author, Received: 30 Nov. 2021, Revised: 01 Feb. 2022, Accepted: 23 Feb. 2022

ABSTRACT: This research aims to investigate the applicability of a fracture simulation method based on a concrete damage model and to construct a framework for evaluating the load capacity of an adhesive post-installed anchor according to a failure mode and load resistant mechanism. A continuum damage model based on the fracture mechanics of semi-brittle materials is used for the simulation and interface elements are set at the boundary between adhesive and concrete. The interface elements are used to simulate the contact state at the fracture boundary. The friction contact model is used to simulate the contact behavior by maintaining the initial stiffness in the direction perpendicular to the interface. As a result, by setting the appropriate friction coefficient and fracture occurrence strain in the interface elements, the combined fracture mode of adhesion and cone fracture, which is a characteristic failure mode of adhesive post-installed anchors, are precisely simulated.

Keywords: Adhesive post-installed anchor, Fracture mechanics, Cone failure mode, Adhesion failure mode, Combined fracture mode

1. INTRODUCTION

Post-installed anchors are a widely used technology for repair and renewal in concrete structures. In recent years, the reliability of the adhesive post-installed anchor has become a social problem in Japan due to accidents such as collapsing ceiling boards in a road tunnel caused by the failure of the adhesive post-installed anchors. Although several organizations have proposed methods for evaluating the performance of post-installed anchors as guidelines and manuals [1]-[4], they have not always been standardized in Japan. In addition, various experiments and studies [e.g.5] have been conducted. However, there are few research cases to evaluate the structural capacity based on a failure mode and load resistant mechanism.

Ryu et al. [6] showed that the failure mode of the adhesive post-installed anchor subjected to uniaxial tension is a combined fracture of cone fracture of the surface layer and adhesion of a deep layer of base material (combined fracture). In addition, Mikura et al. [7] showed that the pull-out strength decreases when the edge distance is 15 times or less of the anchor diameter or when the anchor spacing is 20 times or less of the anchor diameter based on the results of the static pull-out test with parameters as the edge distance and the anchor spacing which evaluate an effect when the anchors are close to each other of when they are close to the edge of the base material. These studies were mainly based on the results of the loading tests, and there is a problem that the crack propagation process inside the base material cannot be understood. It is necessary to construct a numerical simulation method for grasping a damaging process and the progress of microscopic cracks in addition to the experimental approach to construct an evaluation method to understand the damage process and progress of microcracks in addition to the experimental approach.

The study aims to construct a numerical simulation method to evaluate the structural capacity of adhesive post-installed anchors according to the failure mode and load resistant mechanism. Specifically, we verify a reproduction of fracture behavior of the uniaxial pull-out test of the adhesive post-installed anchor as a verification example by Ryu et al. [6], using a continuum damage model based on the fracture mechanics of semi-brittle materials and a damage model considering frictional contact at an interface of damage.

2. FRACTURE SIMULATION METHOD

2.1 Continuum Damage Models Considering Fracture Mechanics of Reinforcing Bars and Concrete

In this research, we verify using a continuum damage model considering fracture mechanics semi-brittle material which is proposed by Kurumatani et al. [8]. The von-Mises plastic model based on the nonlinear isotropic hardening law is applied to reinforcing bars. As shown in Equation (1) and Equation (2), a total strain is additively decomposed into an elastic strain and a plastic strain, and it is assumed that only an elastic component of the stress contributes.

$$\varepsilon = \varepsilon_E + \varepsilon_P \quad (1)$$

$$\sigma = c : \varepsilon_P = c : (\varepsilon - \varepsilon_P) \quad (2)$$

Where ε is the microstrain tensor, ε_E is the elastic strain tensor, ε_P is the plastic strain tensor, σ is the Cauchy stress tensor, and c is the elastic modulus tensor. The yield function as $f \leqq 0$ is adopted by the nonlinear isotropic hardening law given by the exponential function shown in Equation (3).

$$f = \sigma_V - \sigma_{y0} - Q(1 - e^{-bp}) \quad (3)$$

Where, σ_V is the equivalent stress of the Von-Mises, σ_{y0} is the initial yield stress, p is the equivalent plastic strain, and Q and b are parameters for expressing plastic hardening. In addition, the plastic flow rule is followed the related flow rule and is given by Equation (4).

$$d\varepsilon_P = dP \cdot \partial f / \partial \sigma = dpn \quad (4)$$

The isotropic damage model [9] is based on the modified Von-Mises model considering the fracture mechanics of semi-brittle material is applied to the concrete. We model the crack-growth behavior after the elastic limit of concrete. The model used targets the genuine equilibrium problem of the elastic bodies in the process of the damage, and an equilibrium equation, a strain matching condition equation, and each constitutive equation are shown in Equation (5), Equation (6), and Equation (7).

$$\nabla \cdot \sigma + \bar{b} = 0 \quad \text{in } \Omega \quad (5)$$

$$\varepsilon = \frac{1}{2}\{\nabla u + (\nabla u)^T\} \quad \text{in } \Omega \quad (6)$$

$$\sigma = C_D(\varepsilon) \quad \text{in } \Omega \quad (7)$$

Where u is a displacement vector, Ω is an object region, the C_D is a constitutive function considering the damage of the material. In addition, the modified Von-Mises model proposed by De Vree et al. [10] shown in Equation (8) is applied to an equivalent strain ε_{eq}.

$$\varepsilon_{eq} = \frac{k-1}{2k(1-2\nu)} I'_1 + \frac{1}{2k}\sqrt{\left(\frac{k-1}{1-2\nu} I'_1\right)^2 + \frac{12k}{(1+\nu)^2} J'_2} \quad (8)$$

Where ν is the Poisson's ratio, k is compressive tensile strength ratio, I'_1 is the first invariant of a strain tensor, and J'_2 is the second invariant of a deviation strain tensor. The k of the concrete is approximately 10, and substituting this k into Equation (8) can make it possible to express the fracture characteristics that are weak in tension and strong in compression. A relationship between ε_{eq} and an equivalent stress σ_{eq} is expressed by Equation (9), and a damage variable D is expressed as a degree of the damage by $0 \leqq D \leqq 1$. If there is no damage, it will be 0, and if it is destroyed, it will be 1.

$$\sigma_{eq} = [1 - D(\varepsilon_{eq})] E \varepsilon_{eq} = \left[1 - \left\{1 - \frac{\varepsilon_0}{\varepsilon_{eq}} exp\left(-\frac{E\varepsilon_0 h_e}{G_f}(\varepsilon_{eq} - \varepsilon_0)\right)\right\}\right] E \varepsilon_{eq} \quad (9)$$

Where σ_{eq} is equivalent stress, D is a damage variable, ε_0 is a fracture occurrence strain, and h_e is an element length. The damage variable $D(\kappa)$ is expressed assuming that the damage that has occurred is not recovered and the equivalent strain ε_{eq} in the damage variable $D(\varepsilon_{eq})$ is represented by $\kappa \leqq 0$ as the maximum value of the equivalent strain in a deformation history.

$$D(\kappa) = 1 - \frac{\kappa_0}{\kappa} exp\left(-\frac{E\kappa h_e}{G_f}(\kappa - \kappa_0)\right) \quad (10)$$

Where κ_0 is an equivalent strain at the start of the damage. These models are analyzed using the augmentation method and the iterative solution method by the Newton-Raphson method. If a convergent solution cannot be obtained, the modified Newton-Raphson method, which updates the node stiffness for each step, is applied for analysis.

2.2 A Damage Model Considering Contact at a Fracture Boundary

In this research, we decide to reproduce the damage to a boundary near a post-installed anchor that receives a tensile load on the uniaxial using a damage model considering frictional contact of a boundary which was proposed by Soma et al. [10]. The damage model considering the frictional contact at the interface is based on the structural relationship in the local coordinate system and uses a strain ε'_1 in the direction perpendicular to the

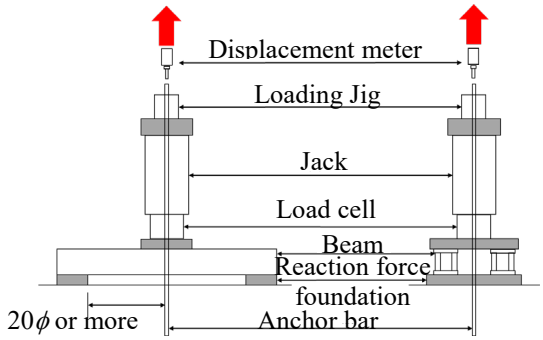

Fig. 1 Loading test equipment [6]

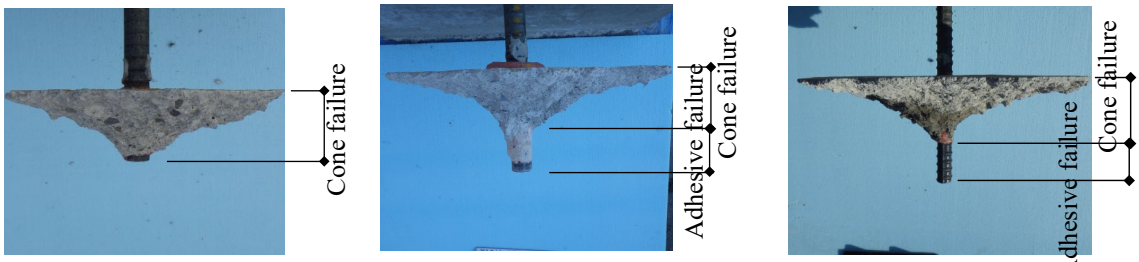

(a) 3ϕ (b) 5ϕ (c) 7ϕ

Fig. 2 Fracture status at the time of pull-out test

interface to determine a contact state of the fracture surface. In case of the fracture surface comes into contact, a contact behavior is expressed by maintaining an initial rigidity in the direction perpendicular to the interface. In addition, Coulomb's friction law is introduced to consider an adhesion and a slippage of the interface in the contact state. Where a friction stress τ_f is expressed by Equation (11) using a stress σ'_1 in the direction perpendicular to the interface.

$$\tau_f = \mu\sigma_n = \mu|\sigma'_1| \tag{11}$$

Where μ is the coefficient of the friction and σ_n is the normal stress. In this model, a shear stress τ'_{12} and τ'_{31} in the local coordinate system are the forces acting along with the interface, and the maximum value of the forces acting along the interface is expressed by Equation (12).

$$\tau'_s = \sqrt{\tau'^2_{12} + \tau'^2_{31}} \tag{12}$$

A slip of the fracture surface is determined comparing τ'_s with the friction stress τ_f. It is assumed that the shear rigidity is equal to the initial rigidity because the fracture surface is fixed in a non-slip state. On the other hand, in the case of a slip state, it is needed to consider shear stress that combines damage and friction because the fracture progresses with frictional slip. A model is shown in Equation (13) which expresses a behavior of the fracture progressing with friction slip is used by combining the shear stress acting on a non-damage area and the frictional stress acting on a damaged area.

$$\tau'_{12} = (1-D)G\gamma'_{12} + D\tau_f \frac{\gamma'_{12}}{\sqrt{\gamma'^2_{12}+\gamma'^2_{31}}}$$
$$\tau'_{31} = (1-D)G\gamma'_{31} + D\tau_f \frac{\gamma'_{31}}{\sqrt{\gamma'^2_{12}+\gamma'^2_{31}}} \tag{13}$$

Where G is the shear rigidity and γ'_{ij} is the strain in the shear direction.

3. EXAMINATION BY THREE DIMENTIONAL ELEMENT ANALYSIS

3.1 Verification Examples

In this research, we decided to use the results of embedded lengths of 3ϕ, 5ϕ, and 7ϕ as verification examples among the uniaxial pull-out tests of the adhesive post-installed anchors conducted by Ryu et al. [6]. Where, ϕ is a diameter of an anchor bar and a D25 which is a deformed bar, was used. Anchor bars were embedded in a concrete specimen whose size is width 900mm × length 900mm × height 500mm, and experiments were conducted

Table 1 Material property of each material [6]

Epoxy resin		Concrete		Anchor bar
σ_{te} (N/mm^2)	σ_{ce} (N/mm^2)	σ_{cc} (N/mm^2)	E_c (kN/mm^2)	σ_{ea} (N/mm^2)
75.7	109	28.5	28.2	1,006

Note: σ_{te} is the tensile strength of the epoxy resin, σ_{ce}

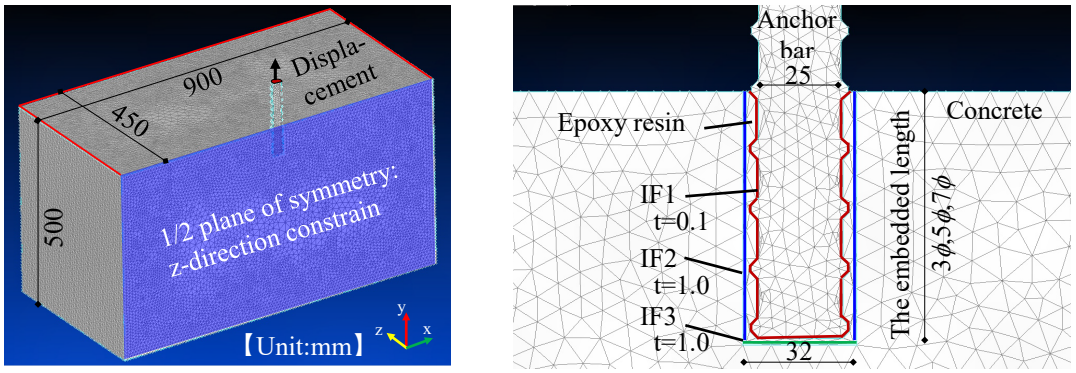

(a) Overall view (b) Detail view

Fig. 3 Outline of analysis model

is the compressive strength of the epoxy resin, σ_{cc} is the compressive strength of the concrete, E_c is the elastic modulus of the concrete, σ_{ea} is the yield strength of the anchor bar.

using a loading test equipment shown in Fig. 1. Table 1 shows the physical characteristics of each material used in the pull-out test. The pull-out tests were performed using 3 specimens in each case.

When the embedded length is 3ϕ as shown in Fig.2(a), caracks were grown diagonally from the bottom tip of the anchor bar and came out in a cone shape, reaching the maximum load (cone failure). The average value of the maximum load at that time was 62.3 kN. When the embedded lengths are 5ϕ and 7ϕ as shown in Fig.2(b) and (c), the cone failure was not formed from the bottom of the anchor bar, however, a cone failure surface was formed from a position of about 4ϕ to 5ϕ from the surface layer of concrete, and a depth of below the concrete failure surface was pulled out by an adhesive failure reaching the maximum load (combined failure). The average vales of the maximum load at those times were 123.9 kN and 193.9kN.

3.2 Outline of an Analysis

Fig.3 shows an outline of an analysis model. The analysis model is defined as a 1/2 symmetric model of the pull-out test specimens. Materials have defined the concrete, the anchor bar, the epoxy resin, an interface element between the anchor bar and the epoxy resin boundary (IF1), an interface element between the epoxy resin on the side surface of the anchor bar and the concrete boundary (IF2), and an interface element between the epoxy resin and the concrete boundary on the bottom of the anchor bar (IF3). Material constitutional rules are used in the analysis are defined as shown in Table 2 concerning the material property values at the time of the experiment shown in Table 1. The fracture energy G_f and ε_0 are defined to sufficiently large values that the anchor bar and the epoxy resin would not be damaged during the analysis.

Elements are meshed by the tetrahedral element, and numbers of the element are 646,009 elements, 660,073 elements, and 652,038 elements, respectively, in the models with the embedded length of 3ϕ, 5ϕ, and 7ϕ. A 1/2 plane of symmetry is constrained Z direction which is its normal direction. In addition, three sides, excluding the side in contact with the 1/2 plane of symmetry, are completely constrained to simulate a reaction force foundation. Displacement of 0.05mm per step is given in the Y direction, and the analysis is performed up to 100 steps.

Table 2 Table of material composition rules

Case	Material composition rules of IF2					
	E (N/mm^2)	ν	μ	k	G_f (N/mm)	ε_0
Case1	28,200	0.2	0.6	13.3	0.0829	7.61E-5
Case2	28,200	0.2	0.1	13.3	0.0829	7.61E-5
Case3	28,200	0.2	1.0	13.3	0.0829	7.61E-5
Case4	28,200	0.2	1.5	13.3	0.0829	7.61E-5
Case5	28,200	0.2	0.6	13.3	0.0829	2.00E-4
Case6	28,200	0.2	0.6	13.3	0.0829	4.00E-4
Case7	28,200	0.2	0.6	13.3	0.0829	6.00E-4

Table 3 Table of analysis cases

Material	E (N/mm^2)	ν	k	G_f (N/mm)	ε_0
Concrete	28,200	0.2	13.3	0.0829	7.61E-5
Anchor bar	200,000	0.3	1.00	1.0000	1.0E+11
Epoxy resin	1,090	0.3	1.44	1.0000	1.0E+11
IF1	28,200	0.3	13.3	1.0000	1.0E+11
IF3	28,200	0.2	100	0.0829	7.61E-5

In this research, an effect on the analysis results is grasped by changing μ and ε_0 of IF2 as shown in Table 3. A notation after here is, e.g., in the case of the Case1 with the embedded length is 3ϕ is written "Case1-3 ϕ".

3.3 Results and Considerations

Fig.4 and Fig.5 show the contour plot of the damage variables at the maximum load in Case1 and Case6. Here, the distribution of the damage variable is exactly the distribution of the damage; however, it can be regarded as an approximate distribution of cracks because an element size is small. Focusing on Fig.4(a), the cracks do not reach the surface layer at the maximum load, although the cracks occur diagonally from the bottom of the anchor bar toward the surface of the concrete, and the maximum load has been reached due to combined failure. Therefore, it is not possible to reproduce the failure behavior during the experiment shown in Fig. 2. Also, focusing on Fig.4(b) and (c), although small cone failures are formed on the concrete surface, the damage is

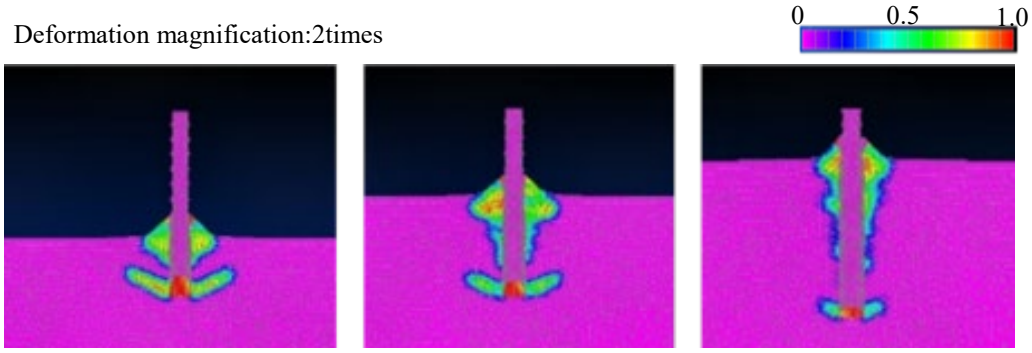

(a) Case1-3ϕ (b) Case1-5ϕ (c) Case1-7ϕ

Fig. 4 Diagram of the damage variable contour

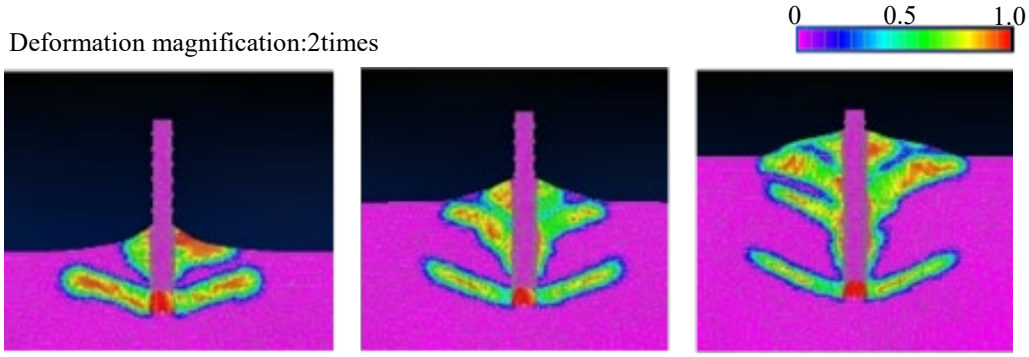

(a) Case6-3ϕ (b) Case6-5ϕ (c) Case6-7ϕ

Fig. 5 Diagram of the damage variable contour

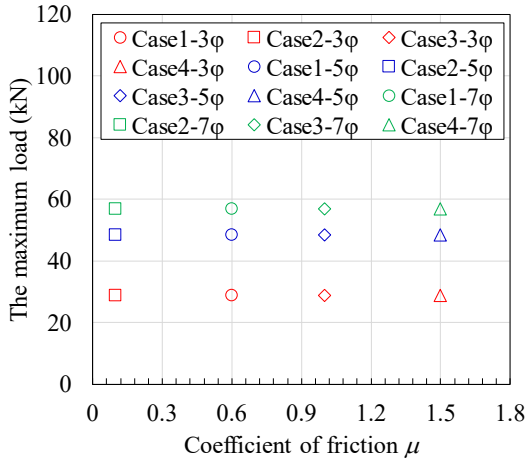

Fig. 6 Relationship between μ and maximum load

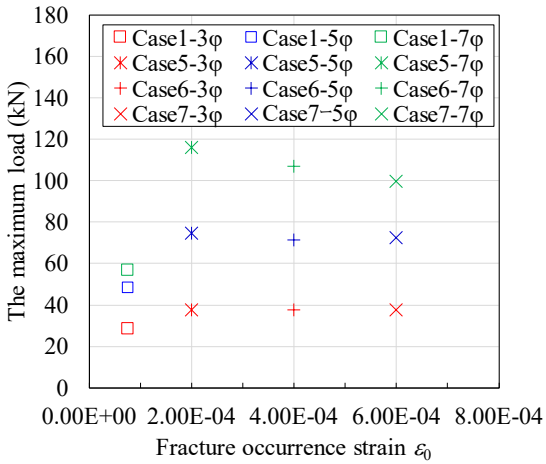

Fig. 7 Relationship between ε_0 and maximum load

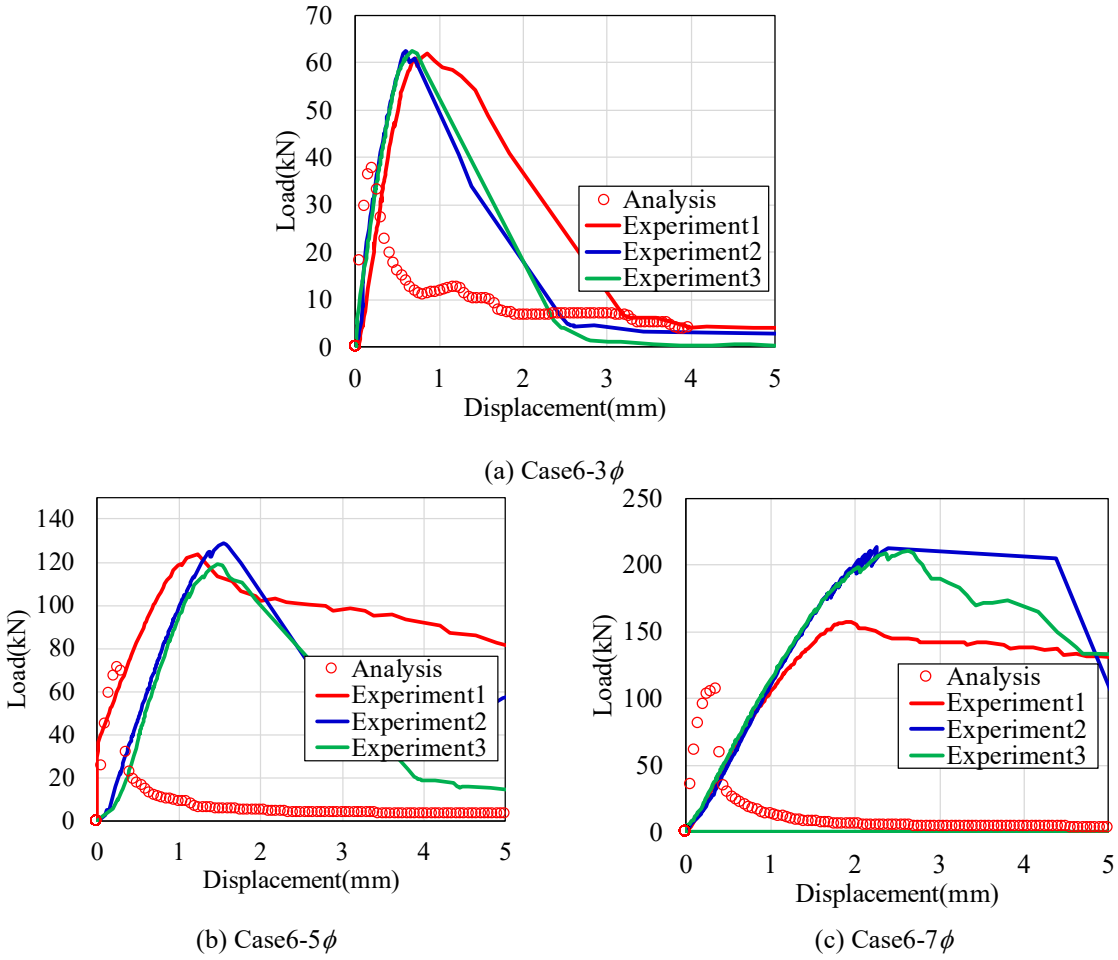

(a) Case6-3ϕ

(b) Case6-5ϕ

(c) Case6-7ϕ

Fig. 8 Relationship between load and displacement in the loading point

concentrated near the interface between epoxy resin and concrete, and cone failure on the surface layer of the concrete reaches the maximum load. Therefore, it is not possible to reproduce the failure behavior during the experiment shown in Fig. 2.

Fig.6 shows the relationship between μ and the maximum load for the analysis results of Case1 to Case4 with varying μ. The maximum load does not change even if the friction coefficient μ is increased. This is thought to be because the shape of IF2 is not uneven, so there is almost no variation in stress in the normal direction. The maximum load value obtained by the analysis is smaller than the maximum load at the time of the experiment, and the analysis cannot be reproduced in the experiment. The distributions of the damage variable from Case2 to Case4 also show approximately the same failure mode, although there was some variation in the size of the small cone failure in the surface layer. Therefore, we have decided to proceed with this research based on the general coefficient of friction between concrete, 0.6.

Fig. 5 shows the damage variation contour at the maximum load in Case6. Focusing on Fig.5 (a), diagonal cracks occur from the bottom of the anchor bar toward the concrete surface and reach the maximum load. Therefore, the failure behavior as cone failure at the time of the experiment shown in Fig.2 can be reproduced. Focusing on Fig.5 (b) and (c), a growth of the cracks in the diagonal direction from the bottom of the anchor bar toward the surface of the concrete can be confirmed however the growth remains inside the concrete. Damage is concentrated near the interface between the epoxy resin and the concrete in the deep part of the anchor bar, and the cone failure on the surface layer of the concrete reaches the surface layer and reaches the maximum load. Therefore, it is possible to reproduce the failure behavior as a combined failure during the experiment shown in Fig. 2.

Fig.7 shows the relationship between ε_0 and the maximum load based on the analysis results of Case1 and Case5 to Case7 with varying ε_0. The maximum load at the time of the analysis increases by increasing ε_0. However, the increase trends are converged when ε_0 exceeds 2E-4. The distribution of the damage variables in Case5 and Case7 were almost the same as the distribution of the damage

variables in Case6 shown in Fig.5. Fig.8 shows relationships between load and displacement in the loading point. In the figure, relationships between load and displacement in the loading point at the time of the experiments are also shown. The maximum loads at the time of the analysis are approximately 50% to 60% of the maximum load at the time of the experiments. And, we focus on initial rigidity. The Case6-3ϕ is almost the same as an initial rigidity at the time of the experiment. On the other hand, the initial rigidities of Case6-5ϕ and Case6-7ϕ tend to be higher than the initial rigidities at the time of the experiments. This was probably due to the elastic deformation of the anchor bar and the elongation of the loading jig during the experiment.

From these results, we show that the failure behavior of the adhesive post-installed anchor can be reproduced roughly by changing the fracture occurrence strain ε_0 of the IF2. On the other hand, we could not reproduce the maximum load at the time of the experiments. In the future, it is going to be necessary to further improve the accuracy of the analysis by considering the fluctuation of the compressive strength according to the restraining effect of the concrete elements in this model.

4. CONCLUSIONS

This study aims to investigate the applicability of a fracture simulation method based on a concrete damage model and to construct a framework for evaluating the load capacity of the adhesive post-installed anchor according to a failure mode and load resistant mechanism. A continuum damage model based on the fracture mechanics of semi-brittle materials is used for the simulation and interface elements are set at the boundary between adhesive and concrete. The interface elements are used to simulate the contact state at the fracture boundary. The friction contact model is used to simulate the contact behavior by maintaining the initial stiffness in the direction perpendicular to the interface. As a result, by setting the appropriate friction coefficient and fracture occurrence strain in the interface elements, the combined failure mode of adhesion and cone failure, which is a characteristic failure form of adhesive post-installed anchors, are precisely simulated.

5. ACKNOWLEDGMENTS

We received kind cooperation from the Railway Technical Research Institute in Japan to the data of the experimental results as a verification example. We would like to express our gratitude to them.

6. REFERENCES

[1] Railway Technical Research Institute in Japan, “ Atosekouanka- no sekkei sekou no tebiki”(The manual of design and construction for the post-installed anchor), 2018

[2] Japan Society of Civil Engineers,”Konkuri-to no atosekouanka-kouhou no sekkei sekou shishin(an)”(The guideline of design and construction for the post-installed anchor in the concrete(Draft)), 2014

[3] Eota, Etag001 Part five: Bonded Anchor, 2013

[4] American Concrete Institute, 355.4-11 Qualification of Post-Installed Anchors in Concrete and Commentary, 2011

[5] e.g. Kazuhito Muramatsu and Eiichi Sou, “Epokishijushianka- no hipparitsuyosa ni kansuru jikkentekikenkyu”(Experimental study on the tensile length for the epoxy resin post-installed anchor), Annual Journal of Japan Concrete Institute, Vol.6, 1984, pp.389-392.

[6] Yuichiro Ryu, Toshiya Tadokoro, Masaru Okamoto and Takutoshi Furuya, Consideration on the pull-out capacity for post-installed anchor based on a load-bearing mechanism, Annual Journal of Japan Concrete Institute, Vol.37, No.2, 2015, pp.505-510.

[7] Hiroaki Mikura, Toshiya Tadokoro, Masaru Okamoto and Yuichiro Ryu, Effects of edge distance and anchor spacing on strength degradation of post-installed bonded anchor, Annual Journal of Japan Concrete Institute, Vol.39, No.2, 2017, pp.463-468.

[8] Mao Kurumatani, Yuki Nemoto, Yuto Soma and Kenjiro Terada, 3D fracture simulation of reinforced concrete based on fracture mechanics for concrete and its performance assessment, Transactions of JSCES, 2016, Paper No.2016004

[9] Mao Kurumatani, Kenjiro Terada, Junji Kato, Takashi Kyoya and Kazuo Kashiyama, An isotropic damage model based on fracture mechanics for concrete and its evaluation, Transactions of JSCES, 2013, Paper No.20130015

[10] J.H.P. de Vree, W.A.M Brekelmans, M.A.J. van Gils : Comparison of nonlocal approaches in continuum damage mechanics, Comput. Struct., 55, 1995, pp.581-588

[11] Yuto Soma and Mao Kurumatani, Fracture simulation of reinforced concrete using damage model considering frictional contact on interface, Journal of JSCE A2 (Applied Mechanics), 75(2), 2019, pp.I_165-I_173.